Physics in Medicine &
Biology

A proof-of-concept automated method for accurate skin dosimetry: correcting overestimated surface dose measurements

Physics in Medicine & Biology

IPEM Institute of Physics and Engineering in Medicine

PAPER

A proof-of-concept automated method for accurate skin dosimetry: correcting overestimated surface dose measurements

Ye-In Park[1], **Hojae Kim**[2], **Se Young Kim**[2], **Junyoung Son**[3], **Changhwan Kim**[1], **Min Cheol Han**[1], **Hojin Kim**[1], **Ho Lee**[1], **Kwang Woo Park**[3], **Dong Wook Kim**[1], **Jin Sung Kim**[1,*] and **Chae-Seon Hong**[1,*]

[1] Department of Radiation Oncology, Yonsei Cancer Center, Heavy Ion Therapy Research Institute, Yonsei University College of Medicine, Seoul, Republic of Korea
[2] Department of Radiation Oncology, Yonsei Cancer Center, Yonsei University Health System, Seoul, Republic of Korea
[3] Department of Radiation Oncology, Yongin Severance Hospital, Yonsei University College of Medicine, Yongin, Gyeonggi-do, Republic of Korea
* Authors to whom any correspondence should be addressed.

E-mail: jinsung@yuhs.ac and cs.hong@yuhs.ac

Keywords: surface dosimetry, skin dose, angular dependence, radiation therapy, detector, optically stimulated luminescence dosimeter, film dosimeter

Supplementary material for this article is available online

OPEN ACCESS

RECEIVED
18 March 2026

REVISED
27 April 2026

ACCEPTED FOR PUBLICATION
28 May 2026

PUBLISHED
16 June 2026

Abstract

Objective. Accurate surface dosimetry is recommended for detecting treatment error and managing skin toxicity. However, measurements using detectors such as optically stimulated luminescence dosimeters (OSLDs) may overestimate surface dose in the buildup region due to detector thickness. We developed a new automated framework to overcome these challenges and enhance dose correction accuracy. *Approach.* The proposed framework includes: (i) determining the detector's position and orientation on the patient's curved surface; (ii) calculating the beam incidence angle for each detector across all radiation beams using treatment planning data and the orientation of the detector; (iii) assessing detector placement relative to the radiation field, and the alignment within irregular subfield areas; (iv) computing the cumulative field contributions to the detector response across all fields; and (v) applying the detector correction factor, defined as the ratio of surface film measurements to detector readings, while considering beam incidence angle and field size. To demonstrate the proof-of-concept of the developed framework, it was evaluated across four treatment modalities using two OSLD types, nanoDot and myOSLchip. Performance was assessed by comparing the OSLD-measured surface dose with the framework-corrected surface dose. *Main results.* The framework effectively corrected OSLD response to reference skin dose, thereby enhancing the accuracy of skin dose estimation. In the anthropomorphic phantom study, the deviation of OSLD response from skin dose varied up to 21.48% for nanoDot and 46.63% for myOSLchip. With the proposed framework, the deviation was reduced to within 5% across all treatment modalities for both OSLD types, demonstrating a substantial improvement in measurement accuracy. *Significance.* This novel framework automates the correction of complex factors affecting surface dosimetry, mitigating measurement variability and improving accuracy and consistency. Its feasibility was demonstrated in a phantom-based, preclinical evaluation using breast radiotherapy treatment plans.

1. Introduction

Accurate *in vivo* surface dosimetry is recommended for effective radiotherapy treatment planning (Noel *et al* 1995, Mijnheer *et al* 2013). Precise surface dose assessment is required to mitigate the development of radiation-induced skin toxicity because the skin is frequently included in the target volume for superficial tumor treatments (Mcdermott 2020). However, skin dose estimation based on planning dose

includes inaccuracies due to dose delivery errors and the limited accuracy in the buildup region reported in many dose calculation algorithms (Court *et al* 2008, Akino *et al* 2013). For ensuring the accurate dose delivered to the skin layer, *in vivo* surface dosimetry during the patient irradiation is a routine procedure in various clinics.

To validate skin dose in clinical practice, direct surface dose measurements using various dosimeters are employed (Jong *et al* 2014, Wagner *et al* 2017, Afereydoon *et al* 2025). Films and optically stimulated luminescence dosimeters (OSLDs) are commonly used for such measurements. While Gafchromic EBT films are suitable for *in vivo* surface dosimetry owing to their thinness, which is comparable to that of the epidermis, their application is limited by their complex dosimetry and delayed readout (Niroomand-Rad *et al* 2020). In contrast, OSLDs offer ease of use, reusability, and rapid readout, making them a practical alternative (Jursinic 2007, Kara and Hicsonmez 2022). However, the waterproof plastic housing of the OSLDs introduces a discrepancy between the actual and measured skin doses (Kry *et al* 2020). In particular, oblique incident beams significantly affect the detector response (DR) in the build-up region (Akbas *et al* 2016). Increasing the incident angle of the beam causes an overresponse in surface dosimetry, the degree of which depends on the water-equivalent thickness of detectors (Apipunyasopon *et al* 2013, Vicoroski *et al* 2017). The difference in response between OSLD and EBT film has been investigated in surface dose measurement, including fluctuations with beam incident angle (Yusof *et al* 2015). Therefore, accurate shallow skin dose estimation from OSLD-based surface dosimetry requires the correction factor optimized for the detector used.

Despite the detector-induced dose discrepancies during surface dosimetry, the method for correcting the DR into the shallow skin dose remains unestablished. Addressing the deviation between DR and dose at the reference skin depth involves overcoming multiple technical challenges and complex procedural requirements. First, the irregular body contours of patients cause surface dosimeters to tilt at various orientations. To account for this, the beam incidence angle correction must be applied individually to detectors based on their orientation. Second, modern radiotherapy techniques deliver doses from multiple gantry angles, making it challenging to analyze the contribution of beam incidence angles to DR. Third, analyzing the detector overresponse requires identifying the fields delivering the dose to each measurement position. In intensity-modulated radiotherapy (IMRT) and volumetric modulated arc therapy (VMAT), correcting detector overresponse is complex, as it involves evaluating both the beam incidence angles and the contribution of irregularly shaped fields.

This study presents a novel framework to estimate dose at the reference skin depth from detector measurements by analyzing factors contributing to overresponse in surface dosimetry. The proposed framework presents a personalized, adaptable, and automated solution to address previously unresolved challenges and uncertainties associated with detector overresponse. The applicability of the developed framework was evaluated using OSLD in an anthropomorphic phantom study with breast radiotherapy plans.

2. Method

This study presents a framework incorporating three key steps to address skin dose overestimation in surface dosimetry (figure 1). The framework integrates treatment planning data with a depth camera-based surface image to automatically calculate the incidence angles of all beams on each detector position. The contributing fields were classified by projecting individual radiation field shapes onto the body surface to determine whether the detector was within an irradiation field. The field-specific correction involved estimating the relative contribution of individual beam fields to the DR across all radiation fields and applying a correction factor based on the beam incidence angle and field size. The correction factor for converting the detector's overresponse to the dose at the reference skin depth was derived from a polynomial curve fitted to the dose difference ratio between the DR and the reference surface dose, as incorporated into the framework. The validity of the developed framework was evaluated using two different OSLD systems, nanoDot (Landauer Inc., Glenwood, IL, USA) and myOSLchip (RadPro International GmbH, Germany), with EBT4 film as the reference for the epidermal skin dose.

2.1. Detector orientation analysis

Identifying the detector position in the coordinates of treatment planning is routine procedure during surface dosimetry for acquiring the planned dose at the measurement location. The proposed framework estimates the detector tilt angle for each detector position by utilizing RT structure data. Surface-normal vectors of external body contour were computed, and then the tilt angle of each detector was defined as

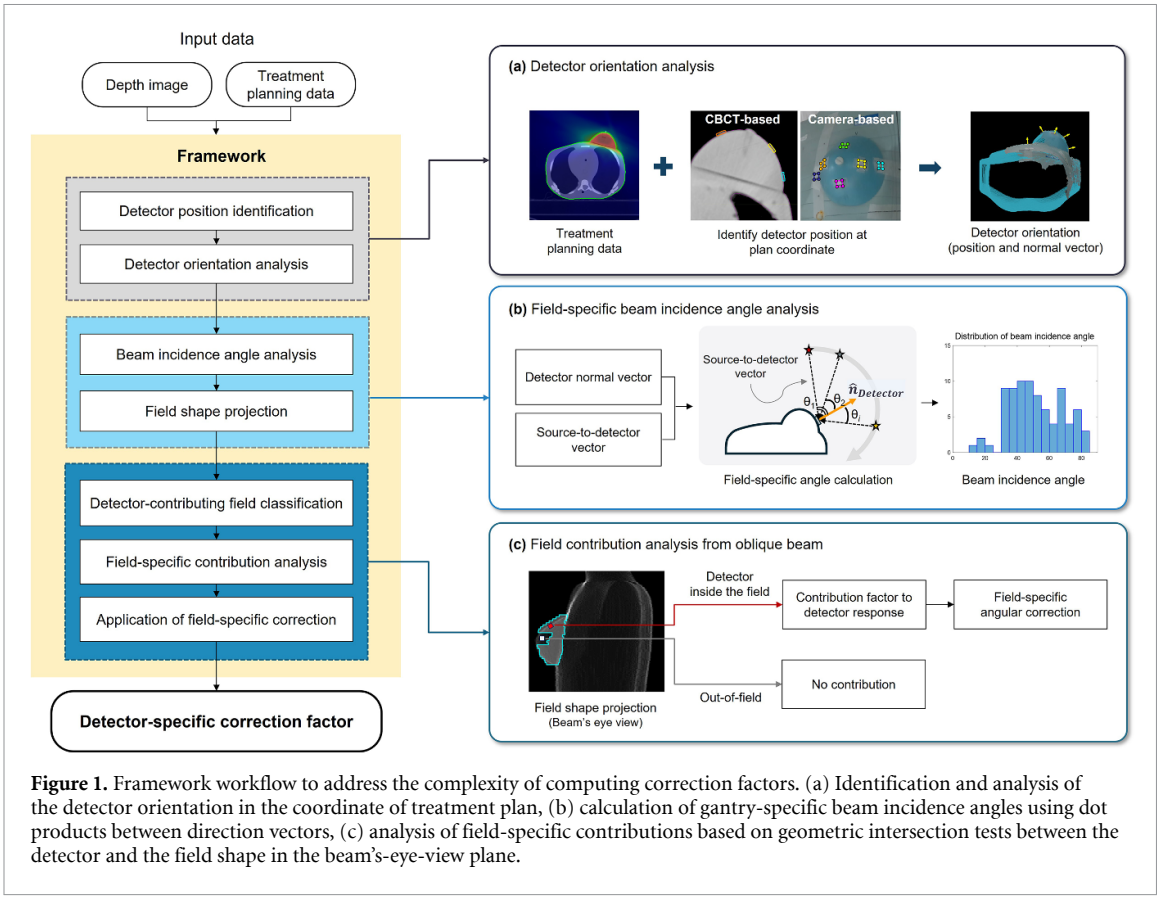

Figure 1. Framework workflow to address the complexity of computing correction factors. (a) Identification and analysis of the detector orientation in the coordinate of treatment plan, (b) calculation of gantry-specific beam incidence angles using dot products between direction vectors, (c) analysis of field-specific contributions based on geometric intersection tests between the detector and the field shape in the beam's-eye-view plane.

the surface-normal vector at the center of the detector position. The detector orientation used to calculate the correction factor consists of detector position and detector tilt angle. The OSLD volume in the framework was defined as a $5 \times 5 \times 2$ mm^3 box placed along the detector orientation and used to identify the beam field contributing to the detectors in the framework.

2.2. Field-specific analysis of beam incident angle and field shape

The beam incidence angle on the detector surfaces was calculated based on the dot product operation between the source-to-detector and the detector orientation vectors. To identify beam contributions to the detector, multileaf collimator (MLC) positions were analyzed at each control point (CP). In DICOM RT files, a CP represents a discrete beam delivery state defined by gantry angle, MLC configuration, and monitor unit (MU) weight, with the total number of CPs determined by the treatment plan. The beam field at the source-to-detector distance was defined by projecting the shape of the beam field along the beam's eye view of each CP. Subsequently, beam field analysis was restricted to CPs where the projected field encompassed the detector's geometric volume. The intersection between the three-dimensional (3D) body surface and the beam delivery path was calculated to evaluate whether the beam incident on the detector was delivered by passing through the body. The source-to-surface distance and equivalent field size were calculated for the point on the entrance surface. The equivalent square for irregularly shaped fields was calculated using the Sterling equation (4 A/P), where A denotes the field area and P its perimeter (Sterling *et al* 1964). This approach was adopted as a practical approximation of field size for surface dose estimation while maintaining computational efficiency within the proposed framework.

2.3. Estimation of relative field contributions to DR

The correction method for overestimated skin dose was developed under the assumption that only CPs with an open field at the detector position contribute to the DR. Given that DICOM dose files typically provide an accumulated dose delivered from multiple CPs, the proposed system includes a procedure to estimate the contribution of individual CPs to the DR. In this approach, an MU-adjusted weighting factor is used to estimate the relative contribution of each irradiation field to the DR, rather than to represent the absolute dose delivered at the detector position. The contribution of each CP to the DR was

estimated based on a MU–to–dose conversion formulation (Gibbons *et al* 2014), as follows:

$$\mathrm{DR_{cp}} = \mathrm{MU_{cp}} \times \mathrm{PDD}\,(r,d) \times \mathrm{WF} \times \mathrm{OF} \times \left(\frac{\mathrm{SCD}}{\mathrm{SSD_{cp}} + \mathrm{d_{max}}}\right)^2 \quad (1)$$

where PDD is the percent depth dose for a $r \times r$ cm^2 field at the depth of measurement d. WF is the wedge factor, and OF is the output factor measured at the surface for different field sizes, normalized to 10×10 cm^2. The remaining is the inverse square factor between the source-to-calibration point distance and the source-to-surface distance.

2.4. Application of field-specific correction factors

In this study, we estimated the skin surface dose from DR using the dose overestimation ratio calculated for each ith CP. The correction factor for overestimated DR ($\mathrm{CF_{Detector}}$) was newly formulated as part of the proposed framework, defined as the ratio of the cumulative DR before and after correction as follows:

$$\mathrm{CF_{Detector}} = \frac{\sum_{i \in CP} \left(\mathrm{DR}_i \cdot \mathrm{AF}\,(\theta_i, r_i)\,|_{\mathrm{entrance}} + \mathrm{DR}_i \cdot \mathrm{BSC}|_{\mathrm{exit}}\right)}{\sum_{i \in CP} \mathrm{DR}_i}, \quad (2)$$

where the AF represents the angle-field correction factor, which adjusts the surface dose difference between the detector overestimation and the dose at the reference skin depth. The AF depends on the incidence angle of the beam (θ) and equivalent square field of $r \times r$ cm^2. Backscatter correction (BSC) factor was applied to the CPs if the detector was located at the exit surface of the beam delivery line. The relative dose reduction at the exit surface of a 10 cm-thick phantom without backscatter material has been reported as 0.81–0.89 for a 6 MV photon beam, depending on the detector used (Kry *et al* 2012, Ponmalar *et al* 2018, Mcdermott 2020). To simplify the correction equation, a representative BSC value of 0.85, corresponding to the midpoint of the reported range, was adopted to minimize selection bias. The overall workflow for CF calculation in the proposed framework is presented in supplementary figure 1.

2.5. Predefinition of angle–field correction factor

The proposed framework requires predefining the AF for the detector being corrected. Herein, we investigated the AF of nanoDot and myOSLchip. The nanoDot consists of a carbon-doped aluminum oxide (Al_2O_3) disk (5 mm diameter $\times$ 0.2 mm thickness) encapsulated in a $10 \times 10 \times 2$ mm plastic housing. In contrast, the myOSLchip is composed of a beryllium oxide (BeO) ceramic ($4.7 \times 4.7 \times 0.5$ mm) housed in a 9.5 mm $\times$ 10 mm $\times$ 2 mm plastic housing. OSLD measurements were performed under controlled conditions in accordance with the recommendations from TG-191 (Kry *et al* 2020). All OSLDs were calibrated under a 6 MV photon beam with 200 MU. The calibration procedure was repeated three times, and only OSLDs with response variability <5% were used in this study. OSLD readout was performed before irradiation to monitor the background signal dose. The measured OSLD dose was calculated as the average of three readouts for each OSLD, subtracted by the background signal. After each experiment, detector bleaching was performed for 14 h for NanoDot and 4 h for MyOSLchip (Jursinic 2007, Kowalski *et al* 2025).

The reference surface dose for determining AF was the Gafchromic^{TM} EBT4 dosimetry film (Ashland, Bridgewater, NJ, USA), which corresponded to the epidermal skin dose. The EBT4 film was cut into 3×3 cm^2 squares for calibration and AF measurements, and 1×1 cm^2 squares for anthropomorphic phantom measurement. The films used in this study were from the same batch, and a small point was drawn on each film cut to indicate the initial orientation of the film. The EBT4 film was calibrated in doses ranging from 30 cGy to 170 cGy. Both OSLDs and film were calibrated at 5 cm depth in a 10 cm stack of water-equivalent solid RW3 slab phantoms (PTW, Freiburg, Germany), using SSD of 100 cm and a field size of 10×10 cm^2. All films were scanned approximately 24 h after irradiation using a Vidar DosimetryPro RED scanner (Vidar Systems Corporation, Herndon, VA, USA) and were stored as a 16-bit, 71 dpi, TIF image.

To minimize the measurement uncertainty for the nanoDot, myOSLchip, and EBT4 films, the consistency of DR was verified. On each measurement day, three samples per detector were randomly selected and irradiated to 50, 100, or 150 cGy under the detector calibration condition. Detectors were considered to require recalibration if the average difference between the delivered doses and measured responses exceeded 5% during this verification procedure. Recalibration of film detectors was planned using film pieces from the same batch, while recalibration of OSLDs was planned to be performed for all samples.

Measurements were conducted using an Elekta Versa HD linear accelerator with a 6 MV photon beam. The output of the linear accelerator was calibrated against a calibrated Farmer-type ionization chamber (TN30013) connected to a UNIDOSE electrometer (PTW-Freiburg, Germany), in accordance with the IAEA TRS-398 protocol (Musolino 2000). The OSLDs and films were placed on the surface of RW3 slabs and aligned at the isocenter. The detectors were irradiated with 300 MU at gantry angles of 0°, 15°, 30°, 45°, 60°, and 75° for field sizes of 3 × 3, 5 × 5, 10 × 10, 15 × 15, and 20 × 20 cm^2. All OSLDs and films were measured three times. The AF of nanoDot and myOSLchip was determined as the average dose ratio between the film and OSLD under identical beam delivery conditions measured on the surface of the RW3 slabs. A polynomial curve was fitted to estimate the AF values of each OSLD at the unmeasured beam incidence angle and field sizes.

2.6. Planning process and performed measurements

We assessed the effectiveness of the framework using the left breast of a female anthropomorphic phantom. Computed tomography (CT) scanning of the phantom was performed with a 2 mm slice thickness (Aquilion One, Canon Medical Systems, Japan). A planning target volume (PTV) was defined for the breast, and the prescribed dose was 50 Gy in 25 fractions. We evaluated the correction accuracy of the framework in relation to beam delivery complexity using four techniques: 3D conformal radiotherapy (3DCRT; 2 CPs, corresponding to two opposing fields), the field-in-field (FiF) technique (6 CPs), IMRT (50 CPs across six beam angles), and VMAT (220 CPs across two arcs).

All treatment plans were generated in accordance with the institutional policy used in this study for breast cancer, without the use of a virtual bolus during plan optimization (Byun *et al* 2021). At least 90% of the PTV received the prescribed dose, while organs at risk met the dose constraints of a mean heart dose $\leqslant$5 Gy and V_{20} <30% for the ipsilateral lung (Kim *et al* 2021). Dose calculation was performed using the collapsed cone convolution algorithm with a dose grid of 2 mm in the RayStation v12 (RaySearch Laboratories AB, Stockholm, Sweden) treatment planning system (TPS).

The measurement points on the phantom surface were defined with markings at six different positions (supplementary figure 2): five on the surface of the breast PTV (positions 1–5) and one on the midsagittal plane (position 6). The detector position on the irregular body surface was determined using an in-house system based on a 3D depth camera, enabling faster localization with accuracy comparable to conventional methods. A 3D depth camera (Intel RealSense D435i; Intel, Santa Clara, CA, USA), which provides both red–green–blue (RGB) color and spatial information, was used to acquire surface images of the phantom with detectors attached. Detector positions were delineated on the RGB surface images and then mapped to the treatment plan coordinate system through 3D surface registration between the acquired images and the patient body contour (Sheen *et al* 2023).

Potential sources of uncertainty in both measurements and framework implementation were addressed through the following procedures. To minimize measurement uncertainty for nanoDot, myOSLchip, and EBT4 film, all measurements were repeated three times on separate days, and DR consistency was verified. On each measurement day, three samples per detector were randomly selected and irradiated to 50, 100, or 150 cGy under calibration conditions. Recalibration was performed if the average difference between delivered doses and measured responses exceeded 5%. Film recalibration was conducted using pieces from the same batch, whereas OSLD recalibration was applied to all samples. Detector misplacement, which affects both measurement and framework-related uncertainties, was minimized by verifying phantom setup reproducibility using cone-beam CT prior to detector placement.

To assess the effectiveness of the OSLD correction factor, dose deviation was computed relative to EBT4 film measurements using the following formula:

$$\text{dose deviation } (\%) = \frac{M_{\text{OSLD}} - M_{\text{Film}}}{M_{\text{Film}}} \times 100, \tag{3}$$

where M_{OSLD} and M_{Film} are the measured dose by OSLD and film at the same detector position, respectively. Dose deviation was assessed for both corrected and uncorrected OSLD measurements. The framework was implemented and evaluated using MATLAB R2023b.

3. Results

A framework was developed and implemented to estimate the epidermal skin dose from overestimated OSLD measurements, converting nanoDot and myOSLchip readings into EBT4 film-equivalent doses. Figure 2 presents the differences in the overresponse ratio between detectors on the surface of the slab phantom. The film responses changed more rapidly than OSLDs as the beam entered obliquely and the

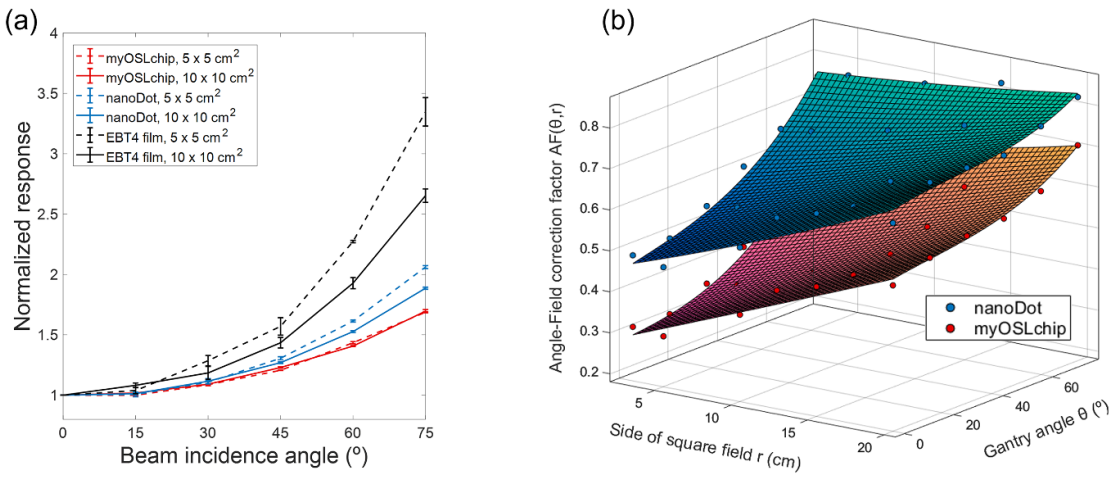

Figure 2. OSLDs surface dose overestimation. (a) Change in detector response from an obliquely incident beam, normalized to the perpendicular beam. (b) Ratios of film dose to OSLD dose as functions of beam incidence angle and equivalent square field size, shown as fitted surfaces for NanoDot (blue) and myOSLchip (pink), along with measured data points.

field size increased. The polynomial curve of AF(θ,r) for nanoDot and myOSLchip was embedded in the developed framework.

An overestimation of surface dose by the OSLDs in the anthropomorphic phantom is summarized in supplementary tables 1 and 2. Dose deviations between OSLD and EBT4 film measurements before framework correction were extensive across the various treatment modalities and detector positions. The mean $\pm$ σ value of the highest dose deviation for nanoDot was 21.48% $\pm$ 1.36% in the IMRT plan, and that for myOSLchip was 46.71% $\pm$ 3.61% in the VMAT plan. These dose deviations between OSLDs and EBT4 film varied depending on the detector position within the same treatment modality. The variation in dose deviation across detector positions was the greatest in the VMAT plan, with a maximum variation of 10.67% for nanoDot (from 7.69% $\pm$ 3.17% to 18.36% $\pm$ 0.81%) and 29.01% for myOSLchip (17.70% $\pm$ 1.61%–46.71% $\pm$ 3.61%).

The framework computed individual OSLD correction factors by analyzing the beam incidence angle for each radiation field contributing to the OSLD measurements (figure 3). Correction factors varied across detector positions, ranging from 0.82 to 0.96 for nanoDot and 0.66–0.87 for myOSLchip. After applying the framework-derived correction factors, the deviation between the surface dose and corrected OSLD measurements was reduced to within 5% for all detector positions, as summarized in figure 4 and supplementary tables 1 and 2.

4. Discussion

A key challenge in surface dosimetry is the discrepancy between DR and shallow skin dose, which is influenced by factors such as beam incidence angle, field size, and detector characteristics. In clinical practice, although high-precision dosimeters can provide accurate reference measurements (Jong *et al* 2014, Wagner *et al* 2017), practical constraints often necessitate the use of more convenient detectors, such as OSLDs, for routine *in vivo* surface dosimetry. However, OSLDs are known to exhibit overresponse in the buildup region, particularly under oblique beam incidence. In this study, we introduced a novel automated method to correct this overestimation by incorporating key factors, including body contour irregularities, beam incidence angle, and the geometric intersection between the beam field and the detector. The proposed framework was successfully applied to estimate the dose at the epidermal layer from nanoDot and myOSLchip responses. Performance evaluations in a phantom-based study using breast radiotherapy plans showed that the average deviation between the corrected OSLD and film responses was <5%, indicating that the proposed framework can accurately correct shallow skin dose overestimation under these conditions. These results suggest that the proposed framework provides consistent performance regardless of the OSLD type, treatment modality, number and complexity of beam incidence angles, or irregularities in the treatment field shape within the context of breast radiotherapy.

Reducing the complexity of beam incidence angle calculation for detectors on curved surfaces is essential for accurate epidermal skin dose estimation from OSLD measurements. Verifying the beam

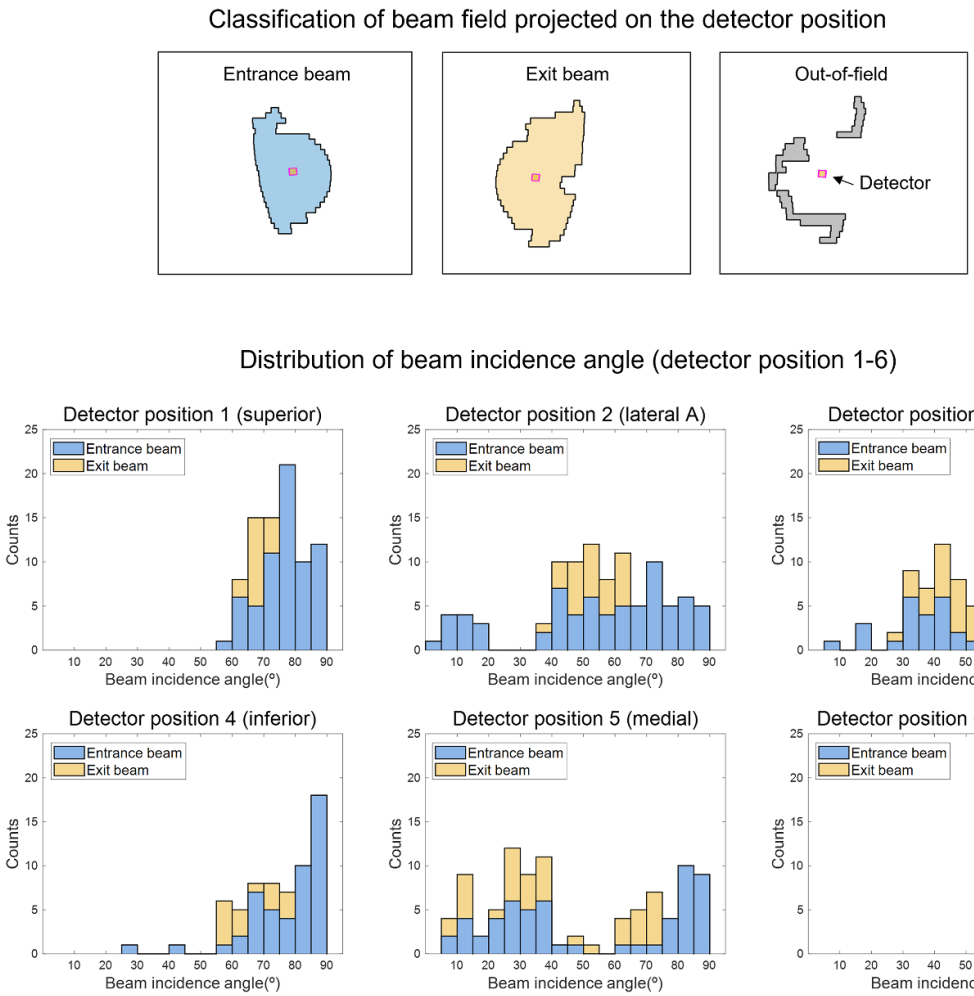

Figure 3. Framework-based analysis of VMAT plan. Beam incidence angles were calculated for fields covering the geometric detector area. Angle distribution varied across six measurement positions (five on the PTV surface, one on the mid-sagittal line).

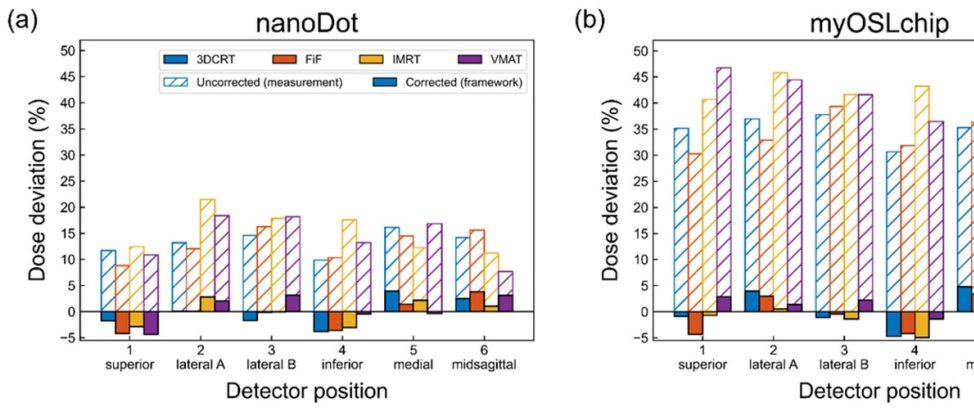

Figure 4. OSLD vs EBT4 film surface dose deviations (uncorrected: hatched, corrected: filled). (a) Nanodot vs EBT4 film, and (b) myOSLchip vs EBT4 film. OSLDs at positions 1–5 are placed on the breast PTV surface, and position 6 is located on the mid-sagittal line. Modalities: 3DCRT, FiF, IMRT, VMAT. Surface dose deviations represent the average of three repeated measurements.

delivery direction for detectors placed on an irregular surface has been performed manually, which is labor-intensive and impractical for complex treatment modalities such as IMRT and VMAT (Tariq *et al* 2019). Consequently, the impact of varying the beam incidence angle distributions on DR has only been analyzed in treatment plans with limited beam delivery angles (Qin *et al* 2014, Yen *et al* 2022). We addressed this limitation by developing a framework that automatically determined the field-specific

beam incidence angle using vector analysis between detector orientation and beam direction at defined CPs. Among the inputs required by the proposed framework, determination of the AF curve is performed only once per beam energy for the film, nanoDot, and myOSLchip systems during initial setup or commissioning and is not repeated during *in vivo* dosimetry measurements. Once established, the AF curve can be reused to calculate a correction factor for subsequent OSLD measurements, eliminating the need for routine film dosimetry during clinical implementation. Factors used for DR calculation, such as PDD, can be acquired through standard clinical procedures, indicating that the framework may be readily applicable. The depth camera-based in-house system used in framework verification was applied to reduce the time spent determining detector orientation, and can be replaced by manual verification of detector placement using CT or cone-beam CT.

Including OSLD and film, the response of passive detectors used for surface dosimetry can be the cumulative value from beam fields irradiated at multiple beam delivery angles. Therefore, contributions from each beam field to the DR should be analyzed for accurate correction of OSLD overresponse. The proposed framework implemented the beam's eye view at the depth of the detector plane to analyze the field size and its contributions to the DR. Analysis of the VMAT treatment plan (figure 3) emphasizes the deviation not only in beam incidence angles but also in the number of fields that directly delivered dose to the detector position. The beam fields classified as out-of-field were not considered in calculating the correction factor from OSLD to film response, to simplify the implementation of the framework. The dose delivered to the surface blocked by the collimator is very low compared to in-field doses; therefore, it may have a negligible impact on the correction accuracy.

The degree of skin dose overestimation caused by beam incidence angle is influenced by the material thickness used in the detector fabrication (Jursinic and Yahnke 2011, Vicoroski *et al* 2017). Previous studies investigated the response of nanoDot to oblique beams in surface dosimetry (Kim *et al* 2012, Yusof *et al* 2015). However, the clinical use of nanoDot for patient measurements is currently limited owing to a manufacturer's recall. The myOSLchip, a newly introduced OSLD, has recently become available for clinical use, whereas the characteristics of the myOSLchip response on surface dose measurement have not yet been investigated. Comparison of OSLD responses measured in a water slab phantom (figure 2) indicates the increase ratio of DR to obliquely incident beam is different for myOSLchip and nanoDot. This discrepancy can be attributed to differences in water-equivalent thickness between the two detectors, as myOSLchip has a water-equivalent thickness of 1.25 mm, compared to 0.4 mm for nanoDot (Yusof *et al* 2015, Sheen *et al* 2023). To account for these differences, the developed framework applies separate correction factors for nanoDot and myOSLchip.

OSLDs overestimate skin doses during breast radiotherapy with two opposing parallel fields (Gopalakrishnan *et al* 2018). However, OSLDs during IMRT have shown that angular-dependent effects are mitigated using multiple beam angles (Zhuang and Olch 2014, Lim-Reinders *et al* 2020). These studies differ from ours in that they compared OSLD measurements to skin doses calculated using a TPS. The TPS-derived skin dose corresponds to the average dose within a dose grid of approximately 2–4 mm, which is thicker than the skin layer defined in this study (Cao *et al* 2017, Wang *et al* 2018, Park *et al* 2022). In our study, OSLD measurements similarly followed the trend of TPS-derived surface dose at a 2 mm depth (supplementary figure 3). Given the limitations of TPS in terms of accurately calculating skin doses, comparing OSLD measurements with EBT4 film (approximately 0.153 mm thick) offers more reliable information about OSLD overestimation (Akbas *et al* 2016). The mean dose deviation between OSLD and EBT4 film measurements reached 46.71% for myOSLchip and 21.48% for nanoDot, emphasizing the necessity of correction for overresponse to ensure accurate OSLD-based skin dose validation.

The definition and clinical significance of skin thickness may vary depending on the treatment site, therapeutic goal, type of toxicity, and clinician's judgment (Johansen *et al* 1996, FitzGerald *et al* 2008, Hong *et al* 2024). This study used film measurements as a reference for the actual skin dose, as their effective thickness is similar to the basal layer, which is the most acutely responsive part of skin to radiation damage (Kim *et al* 2013). Conversely, some studies have evaluated the skin dose at depths of 2–4 mm, considering the relationship between the radiation response and the dose to the epidermis and dermis in the manifestation of chronic symptoms (Hirota *et al* 2002, Rübe *et al* 2024). Therefore, caution should be exercised when directly applying our results in clinical practice. Nevertheless, the proposed framework allows users to modify a reference skin depth by replacing the film with another dosimeter during AF curve fitting, thus enabling the estimation for various clinically relevant skin thicknesses. The measurement procedure of the detector corresponding to reference skin depth would only be required once for determining the AF curve, which can be effective for estimating the dose at various skin depths from surface dosimetry based on OSLD measurements.

All measurements inherently involve uncertainty. Accordingly, we adopted careful calibration and measurement procedures to minimize uncertainty in the measured results. The uncertainty of nanoDot OSLD measurements was estimated to be 3.5%–4.9% at the 1σ level, as the OSLD measurements were performed in accordance with the recommendations of TG-191 (Kry *et al* 2020). The total uncertainty in film dosimetry arising from measurement and calibration, was estimated to range from 3.50% to 4.55% using the formulation proposed by Devic *et al* (2016). Through additional verification of both OSLDs and film, this study maintained the uncertainty associated with DR–to–dose conversion below 5% across all measurements. Uncertainty due to detector misplacement was considered negligible, as detector positioning was controlled using a cone-beam CT–based phantom setup in conjunction with surface markings. Nevertheless, within the proposed framework, accurate determination of detector position remains important because it directly affects estimation of the detector normal vector and the corresponding correction factors. Notably, this study represents a proof of concept; therefore, future work will focus on systematically evaluating sources of uncertainty within the framework and developing strategies to mitigate their impact in practical clinical applications. The main sources of uncertainty in this study are summarized as follows: (i) measurement uncertainties associated with the calibration and measurement of OSLDs and film; (ii) detector positioning uncertainty affecting the estimation of detector orientation; and (iii) framework-related uncertainties, including AF curve fitting and geometric assumptions in the correction process.

Although the proposed framework demonstrated promising results, it has certain limitations. First, its generalizability has not been thoroughly evaluated. Further validation is required to assess its applicability across different beam energies and treatment sites. Second, the framework was validated using an anthropomorphic phantom to demonstrate the proof-of-concept, but has not yet been tested on actual patients in a clinical setting. This limitation indicates that the parameters and strategies implemented within the framework may not inherently yield optimal clinical outcomes. Third, differences in detector thickness between OSLDs and EBT4 film may introduce geometric discrepancies near the field edge, where the film may be included within the irradiation field while the OSLD is excluded for certain IMRT or VMAT beam segments. Because the framework's accuracy was assessed through comparison with film-based reference doses, such discrepancies may have influenced the phantom study results. Finally, this study primarily focused on OSLD over-response owing to the buildup effect, and certain parameters influencing DR were simplified or omitted to balance computational efficiency and accuracy. Incorporating optimization of the BSC value, along with additional corrections such as off-axis ratio and out-of-field dose contributions (Kry *et al* 2012), may further improve the accuracy of film-equivalent dose estimation in OSLD-based surface dosimetry.

5. Conclusions

We successfully developed a novel automated framework to estimate skin dose at a reference depth by correcting overestimated surface dosimetry measurements. This framework provides a systematic approach to address previously intractable challenges and uncertainties related to DR differences in surface dosimetry. The feasibility evaluation using two commercial OSLDs in an anthropomorphic phantom study demonstrated that the proposed method has flexible components that can be refined based on detector characteristics. Our framework effectively reduced surface dose overestimation in OSLD measurements by automating corrections for angle and field size dependence. This study highlights the importance of a personalized and automated approach that accounts for both detector characteristics and treatment modalities to achieve accurate epidermal dosimetry. Further studies are required to validate these findings in clinical patients and to assess the broader applicability of this approach across different treatment sites.

Acknowledgments

This work was supported by the National Research Foundation of Korea(NRF) Grant funded by the Korea Government(MSIT) (RS-2024-00455777) and by a Severance Hospital Research fund for Clinical excellence (SHRC) (C-2025-0001).

Data availability statement

All data that support the findings of this study are included within the article (and any supplementary information files).

Supplementary data 1 available at: https://doi.org/10.1088/1361-6560/ae74b1/data1.

Conflict of interest

The authors have no relevant conflicts of interest to disclose.

Author contributions

Ye-In Park
Data curation (equal), Formal analysis (lead), Investigation (lead), Methodology (lead), Software (lead), Validation (supporting), Visualization (lead), Writing – original draft (equal), Writing – review & editing (supporting)

Hojae Kim
Investigation (supporting), Validation (supporting), Writing – review & editing (supporting)

Se Young Kim
Investigation (supporting), Validation (supporting), Writing – review & editing (supporting)

Junyoung Son
Investigation (supporting), Validation (supporting), Writing – review & editing (supporting)

Changhwan Kim 0000-0003-0050-0470
Methodology (supporting), Resources (supporting), Writing – review & editing (supporting)

Min Cheol Han 0000-0002-1465-5636
Methodology (supporting), Resources (supporting), Writing – review & editing (supporting)

Hojin Kim 0000-0002-4652-8682
Methodology (supporting), Resources (supporting), Writing – review & editing (supporting)

Ho Lee 0000-0001-5773-6893
Methodology (supporting), Resources (supporting), Writing – review & editing (supporting)

Dong Wook Kim
Methodology (supporting), Resources (supporting), Writing – review & editing (supporting)

Jin Sung Kim 0000-0003-1415-6471
Project administration (lead), Writing – review & editing (lead)

Chae-Seon Hong 0000-0001-9120-6132
Conceptualization (lead), Data curation (equal), Formal analysis (supporting), Funding acquisition (lead), Investigation (lead), Methodology (lead), Project administration (lead), Resources (lead), Software (supporting), Supervision (lead), Validation (lead), Visualization (supporting), Writing – original draft (equal), Writing – review & editing (lead)

References

Afereydoon S, Enferadi-Aliabad M J, Gholizadeh M, Rezaei Y, Broomand M A, Daneshfar R and Nickfarjam A 2025 Comparative surface dosimetry in breast cancer in 3DCRT radiotherapy: TLD measurements and TPS evaluation across techniques *Radiat. Phys. Chem.* **229** 112559

Akbas U, Donmez Kesen N, Koksal C and Bilge H 2016 Surface and buildup region dose measurements with markus parallel-plate ionization chamber, GafChromic EBT3 Film, and MOSFET detector for high-energy photon beams *Adv. High Energy Phys.* **2016** 8361028

Akino Y, Das I J, Bartlett G K, Zhang H, Thompson E and Zook J E 2013 Evaluation of superficial dosimetry between treatment planning system and measurement for several breast cancer treatment techniques *Med. Phys.* **40** 011714

Apipunyasopon L, Srisatit S and Phaisangittisakul N 2013 An investigation of the depth dose in the build-up region, and surface dose for a 6-MV therapeutic photon beam: Monte Carlo simulation and measurements *J. Radiat. Res.* **54** 374–82

Byun H K et al 2021 Risk of lymphedema following contemporary treatment for breast cancer: an analysis of 7617 consecutive patients from a multidisciplinary perspective *Ann. Surg.* **274** 170–8
Cao Y, Yang X, Yang Z, Qiu X, Lv Z, Lei M, Liu G, Zhang Z and Hu Y 2017 Superficial dose evaluation of four dose calculation algorithms *Radiat. Phys. Chem.* **137** 23–28
Court L E, Tishler R B, Allen A M, Xiang H, Makrigiorgos M and Chin L 2008 Experimental evaluation of the accuracy of skin dose calculation for a commercial treatment planning system *J. Appl. Clin. Med. Phys.* **9** 29–35
Devic S, Tomic N and Lewis D 2016 Reference radiochromic film dosimetry: review of technical aspects *Phys. Med.* **32** 541–56
Fitzgerald T J et al 2008 Radiation therapy toxicity to the skin *Dermatol. Clin.* **26** 161–72
Gibbons J P, Antolak J A, Followill D S, Huq M S, Klein E E, Lam K L, Palta J R, Roback D M, Reid M and Khan F M 2014 Monitor unit calculations for external photon and electron beams: report of the AAPM therapy physics committee task group no. 71 *Med. Phys.* **41** 031501
Gopalakrishnan Z, Nair R, Raghukumar P, Menon S and Bhasi S 2018 Verification of treatment planning algorithms using optically stimulated luminescent dosimeters in a breast phantom *J. Med. Phys.* **43** 264–9
Hirota S, Tsujino K, Oshitani T, Hishikawa Y, Takada Y, Kono M and Abe M 2002 Subcutaneous fibrosis after whole neck irradiation *Int. J. Radiat. Oncol. Biol. Phys.* **52** 937–43
Hong C-S et al 2024 Dose–toxicity surface histogram-based prediction of radiation dermatitis severity and shape *Phys. Med. Biol.* **69** 115041
Johansen J, Bentzen S M, Overgaard J and Overgaard M 1996 Relationship between the *in vitro* radiosensitivity of skin fibroblasts and the expression of subcutaneous fibrosis, telangiectasia, and skin erythema after radiotherapy *Radiother. Oncol.* **40** 101–9
Jong W L, Wong J H D, Ung N M, Ng K H, Ho G F, Cutajar D L and Rosenfeld A B 2014 Characterization of MOSkin detector for *in vivo* skin dose measurement during megavoltage radiotherapy *J. Appl. Clin. Med. Phys.* **15** 120–32
Jursinic P A 2007 Characterization of optically stimulated luminescent dosimeters, OSLDs, for clinical dosimetric measurements *Med. Phys.* **34** 4594–604
Jursinic P A and Yahnke C J 2011 *In vivo* dosimetry with optically stimulated luminescent dosimeters, OSLDs, compared to diodes; the effects of buildup cap thickness and fabrication material *Med. Phys.* **38** 5432–40
Kara E and Hicsonmez A 2022 Physical and dosimetric characteristic properties of BeO OSL for clinical dosimetric measurements *Appl. Radiat. Isot.* **186** 110199
Kim D W et al 2012 Dose response of commercially available optically stimulated luminescent detector, Al_2O_3: c for megavoltage photons and electrons *Radiat. Prot. Dosim.* **149** 101–8
Kim J H, Kolozsvary A J J, Jenrow K A and Brown S L 2013 Mechanisms of radiation-induced skin injury and implications for future clinical trials *Int. J. Radiat. Biol.* **89** 311–8
Kim N, Chang J S, Shah C, Shin H, Keum K C, Suh C-O and Kim Y B 2021 Hypofractionated volumetric-modulated arc therapy for breast cancer: a propensity-score-weighted comparison of radiation-related toxicity *Int. J. Cancer* **149** 149–57
Kowalski J P, Erickson B G, Wu Q, Li X and Yoo S 2025 Characterization, commissioning, and clinical evaluation of a commercial BeO optically stimulated luminescence (OSL) system *J. Appl. Clin. Med. Phys.* **26** e70057
Kry S F et al 2020 AAPM TG 191: clinical use of luminescent dosimeters: tLDs and OSLDs *Med. Phys.* **47** e19–e51
Kry S F, Smith S A, Weathers R and Stovall M 2012 Skin dose during radiotherapy: a summary and general estimation technique *J. Appl. Clin. Med. Phys.* **13** 20–34
Lim-Reinders S, Keller B M, Sahgal A, Chugh B and Kim A 2020 Measurement of surface dose in an MR-Linac with optically stimulated luminescence dosimeters for IMRT beam geometries *Med. Phys.* **47** 3133–42
Mcdermott P N 2020 Surface dose and acute skin reactions in external beam breast radiotherapy *Med. Dosim.* **45** 153–8
Mijnheer B, Beddar S, Izewska J and Reft C 2013 *In vivo* dosimetry in external beam radiotherapy *Med. Phys.* **40** 070903
Musolino S V 2000 Absorbed dose determination in external beam radiotherapy: an international code of practice for dosimetry based on standards of absorbed dose to water *Technical Reports Series* No. 398 (IAEA)
Niroomand-Rad A et al 2020 Report of AAPM task group 235 radiochromic film dosimetry: an update to TG-55 *Med. Phys.* **47** 5986–6025
Noel A, Aletti P, Bey P and Malissard L 1995 Detection of errors in individual patients in radiotherapy by systematic *in vivo* dosimetry *Radiother. Oncol.* **34** 144–51
Park Y-I, Choi S H, Hong C-S, Cho M-S, Son J, Jang J W, Kim J, Kim H, Kim D W and Kim J S 2022 A pilot study of a novel method to visualize three-dimensional dose distribution on skin surface images to evaluate radiation dermatitis *Sci. Rep.* **12** 2729
Ponmalar R, Manickam R, Saminathan S, Ganesh K M, Raman A and Godson H F 2018 Evaluation of optically stimulated luminescence dosimeter for exit dose *in vivo* dosimetry in radiation therapy *J. Cancer Res. Ther.* **14** 1341–9
Qin S, Chen T, Wang L, Tu Y, Yue N and Zhou J 2014 Angular dependence of the MOSFET dosimeter and its impact on *in vivo* surface dose measurement in breast cancer treatment *Technol. Cancer Res. Treat.* **13** 345–52
Rübe C E, Freyter B M, Tewary G, Roemer K, Hecht M and Rübe C 2024 Radiation dermatitis: radiation-induced effects on the structural and immunological barrier function of the epidermis *Int. J. Mol. Sci.* **25** 3320
Sheen H et al 2023 Novel framework for determining TPS-calculated doses corresponding to detector locations using 3D camera in *in vivo* surface dosimetry *Phys. Med. Biol.* **68** 055011
Sterling T D, Perry H and Katz L 1964 Automation of radiation treatment planning—IV. Derivation of a mathematical expression for the per cent depth dose surface of cobalt 60 beams and visualisation of multiple field dose distributions *Br. J. Radiol.* **37** 544–50
Tariq M, Gomez C and Riegel A C 2019 Dosimetric impact of placement errors in optically stimulated luminescent *in vivo* dosimetry in radiotherapy *Phys. Imaging Radiat. Oncol.* **11** 63–68
Vicoroski N et al 2017 Development of a silicon diode detector for skin dosimetry in radiotherapy *Med. Phys.* **44** 5402–12
Wagner D M, Hüttenrauch P, Anton M, von Voigts-rhetz P, Zink K and Wolff H A 2017 Feasibility study of entrance and exit dose measurements at the contra lateral breast with alanine/electron spin resonance dosimetry in volumetric modulated radiotherapy of breast cancer *Phys. Med. Biol.* **62** 5462
Wang L, Cmelak A J and Ding G X 2018 A simple technique to improve calculated skin dose accuracy in a commercial treatment planning system *J. Appl. Clin. Med. Phys.* **19** 191–7

Yen T-Y, Chuang K-C, Fu H-M, Feng C-J, Lien K-Y and Hsu S-M 2022 Estimation of the surface dose in breast irradiation by the beam incident angle and the 1 cm depth dose *J. Clin. Med.* **11** 2154

Yusof F H, Ung N M, Wong J H D, Jong W L, Ath V, Phua V C E, Heng S P and Ng K H 2015 On the use of optically stimulated luminescent dosimeter for surface dose measurement during radiotherapy *PLoS One* **10** e0128544

Zhuang A H and Olch A J 2014 Validation of OSLD and a treatment planning system for surface dose determination in IMRT treatments *Med. Phys.* **41** 081720